Research Article

Journal of Environmental Nanotechnology

Performance Evaluation of Nano TiO_2–basalt Fiber Hybrid Geopolymers: Mechanical Response, Long-term Durability, and Metal Immobilization Efficiency

M. Nanthini[1], V. Jaganathan[1*] and R. Vinodhini[2]

[1]Department of Civil Engineering, Saveetha School of Engineering, Saveetha Institute of Medical and Technical Sciences, Chennai, TN, India
[2]Department of Mathematics, Saveetha School of Engineering, Saveetha Institute of Medical and Technical Sciences, Chennai, TN, India
Received: 11.01.2026 Accepted: 16.02.2026 Published: 30.03.2026
* Jagnthan@gmail.com

ABSTRACT

Geopolymers have emerged as promising low-carbon alternatives to Portland cement. However, their quasi-brittle behavior and sensitivity to microcracking limit broader structural adoption. This study investigates the synergistic effects of basalt fiber and TiO_2 nanoparticle reinforcement on the mechanical, durability, microstructural, and leaching performance of fly ash–slag based geopolymers. The novelty of this study lies in the synergistic integration of nano- TiO_2 with basalt fiber reinforcement in geopolymer matrices, enabling simultaneous enhancement of mechanical performance, durability, and heavy-metal immobilization within a single sustainable composite system. Five mix formulations were prepared with varying basalt fiber volume fractions (0–1.0%) and TiO_2 nanoparticle dosages (0–2.0%). Comprehensive characterization, including compressive, flexural, and tensile testing; permeability, acid/sulfate exposure, freeze–thaw cycling; SEM, XRD, FTIR analyses; and TCLP-based leachate evaluation, was conducted. Results show that TiO_2 incorporation substantially refines the matrix through accelerated geopolymerization and pore densification, while basalt fibers enhance crack bridging, tensile resistance, and structural stability. The hybrid mix containing 1.0% basalt fiber and 1.0% TiO_2 (GP-B1T1) exhibited the best performance, with compressive strength exceeding 68 MPa, reduced sorptivity (≈0.19 mm/min$^{1/2}$), minimal freeze–thaw damage, superior chemical resistance, and up to 30% reduction in heavy metal leaching compared to the control. Microstructural analyses confirmed the formation of a highly compacted gel network with strong fiber–matrix bonding and minimal microdefects. These findings demonstrate that multi-scale reinforcement using TiO_2 nanoparticles and basalt fibers can significantly elevate the structural reliability, durability, and environmental stability of geopolymer composites, making them as viable candidates for sustainable infrastructure applications.

Keywords: Geopolymer composites; Basalt fiber reinforcement; TiO_2 nanoparticles; Durability performance; Microstructural characterization; Heavy metal immobilization

1. INTRODUCTION

The construction industry is at a critical juncture, facing the dual challenges of meeting global infrastructure demands and mitigating its substantial environmental footprint (Vignesh *et al*. 2025). Portland cement, the binder in conventional concrete, is responsible for approximately 8% of global anthropogenic CO_2 emissions, primarily due to the calcination process and high energy requirements of its production (Vignesh *et al*. 2025). This environmental imperative has catalysed the search for sustainable, low-carbon alternative binders. Among these, geopolymers have emerged as a leading candidate. Formed by the alkaline activation of aluminosilicate precursors like fly ash or ground granulated blast furnace slag (GGBS), geopolymers offer a promising pathway to reduce embodied carbon by up to 80% compared to ordinary Portland cement, while also valorising industrial by-products (Vignesh *et al*. 2025). While geopolymers exhibit excellent compressive strength, thermal stability, and early-age properties, their quasi-brittle nature and susceptibility to microcracking under tensile or flexural loads limit their broader structural application (Nanthini *et al*. 2024). Furthermore, long-term durability in aggressive environments and the potential leaching of heavy metals from certain industrial by-products are areas requiring detailed investigation (Xu *et al*. 2025). To overcome these limitations, researchers have explored various reinforcement strategies. Fiber reinforcement, particularly with sustainable mineral fibers like basalt, has proven effective in bridging microcracks, improving tensile and flexural strength, and enhancing fracture toughness (John *et al*. 2021). The integration of nanoparticles offers a complementary strategy for matrix-level refinement. TiO_2 nanoparticles, for instance, are known to act as nano-fillers and nuclei for geopolymerization, leading to a denser, more homogeneous microstructure with reduced porosity, which can significantly improve mechanical performance and durability (Raza *et al*. 2023).

However, the synergistic interaction between macro-scale fiber reinforcement (basalt fiber) and nano-

scale particle modification (TiO_2) within a geopolymer matrix remains underexplored. The potential for basalt fibers to provide toughening mechanisms while TiO_2 nanoparticles enhance the matrix quality and fiber-matrix interfacial bond could unlock superior composite performance. Moreover, the environmental safety of such novel composites, particularly their leaching behavior, is a critical parameter for sustainable material approval that has not been comprehensively addressed for this specific hybrid system.

Therefore, this study aims to fill this knowledge gap by developing and systematically evaluating a novel geopolymer composite reinforced with hybrid basalt fibers and TiO_2 nanoparticles. The research employs a comprehensive experimental programme to: (i) assess the synergistic effects on mechanical properties, including compressive, flexural, and splitting tensile strength; (ii) evaluate key durability indicators such as water sorptivity, acid/sulfate resistance, and freeze-thaw performance; and (iii) critically analyse the leaching characteristics of the developed composites to ensure their environmental compatibility. By integrating mechanical, microstructural, durability, and environmental analyses, this work provides a holistic assessment necessary for advancing the practical application of high-performance, sustainable geopolymer composites in modern construction.

2. MATERIALS AND METHODS

2.1 Materials

The geopolymer binder was formulated using two principal aluminosilicate precursors. Class F fly ash, compliant with ASTM C618, was sourced from the Neyveli Thermal Power Station, Tamil Nadu, India. X-ray fluorescence (XRF) analysis confirmed its primary chemical composition as 51.8% SiO_2, 27.3% Al_2O_3 and 10.1% Fe_2O_3. Ground granulated blast furnace slag was procured from JSW Steel, Bellary, India to enhance early strength development and refine the pore structure. The alkaline activator consisted of a combination of laboratory-grade sodium hydroxide pellets and a commercial sodium silicate solution with a SiO_2/Na_2O mass ratio of 2.2 and 63% water content. The activator solution was prepared 24 hours prior to mixing and stored at ambient temperature.

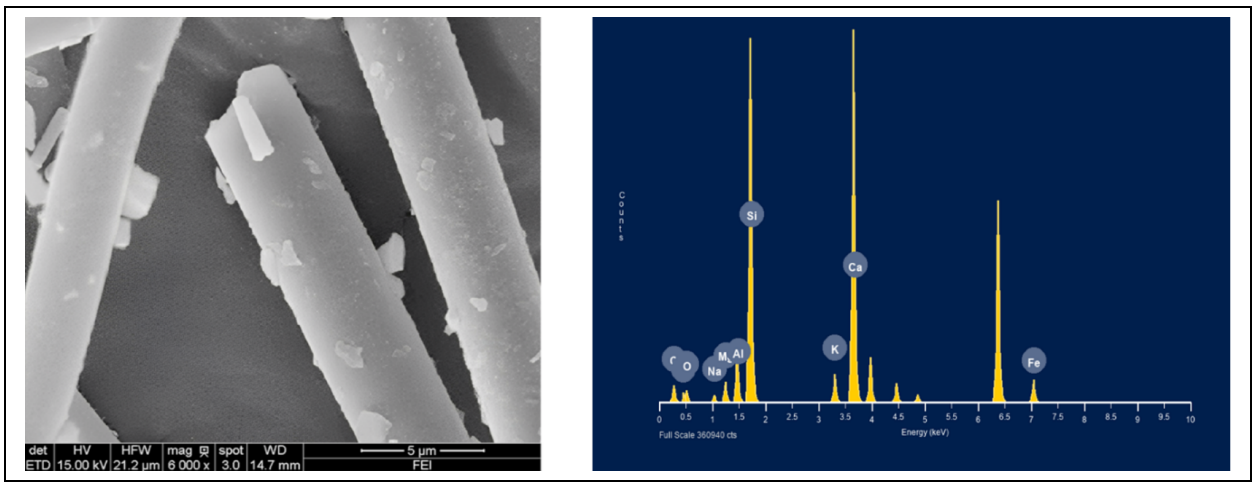


Fig. 1: SEM/EDX analyses of basalt fibers

For reinforcement, chopped basalt fibers with a length of 12 mm and a nominal diameter of 17 µm were obtained from commercial Sources. The fibers possessed a tensile strength of 3.1 GPa and an elastic modulus of 95 GPa. Their microstructural characteristics were derived using SEM/EDX (Fig 1). The TiO_2 nanoparticles were synthesized via a sol-gel process detailed in Section 2.1.1. Deionized water was used throughout the experimental program.

2.1.1 Synthesis of TiO_2 Nanoparticles

TiO_2 nanoparticles were synthesized using a modified acid-catalyzed sol-gel method. Titanium isopropoxide (TTIP, 97% purity, Sigma-Aldrich) was used as the titanium precursor. In a typical synthesis, 20 ml of TTIP was added dropwise under vigorous stirring to 200 mL of deionized water maintained at 60°C. The pH of the solution was adjusted to 2.0 using concentrated nitric acid to catalyze the hydrolysis reaction. The resulting mixture was continuously stirred for 3 hours to form a stable, translucent sol. This sol was then subjected to hydrothermal treatment in a Teflon-lined autoclave at 180°C for 12 hours. The resultant precipitate was centrifuged, washed repeatedly with deionized water and ethanol to remove impurities, and finally dried at 80°C for 24 hours. The dried powder was calcined at 450°C for 2 hours in a muffle furnace to obtain crystalline anatase-phase TiO_2 nanoparticles. The synthesized nanoparticles were characterized using SEM microscopy and Energy Diffraction Spectroscopy as shown in Fig 2, confirming an average crystallite size and a spherical morphology.

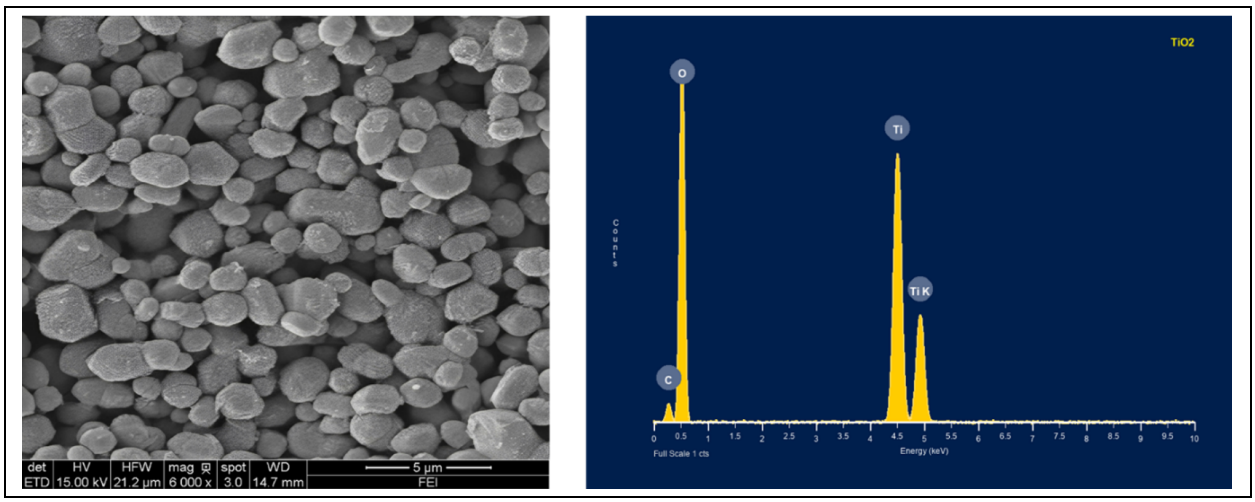


Fig. 2: SEM/EDX analyses of TiO_2 nanoparticles

2.2 Specimen Preparation and Curing

Five distinct mix compositions were designed, as detailed in Table 1. The control mix, designated GP-C, contained no reinforcement. The modified composites incorporated basalt fibers at 0.5% and 1.0% by volume and TiO_2 nanoparticles at 1.0% and 2.0% by weight of the total solid precursors (fly ash + slag).

Table 1. Mix proportions of geopolymer composites (quantities in kg/m³)

Mix ID	Fly Ash	GGBS	NaOH	Na_2SiO_3	BF (vol.%)	TiO_2 (wt.%)
GP-C	450	150	48	120	0.0	0.0
GP-T1	450	150	48	120	0.0	1.0
GP-B05T1	450	150	48	120	0.5	1.0
GP-B1T1	450	150	48	120	1.0	1.0
GP-B1T2	450	150	48	120	1.0	2.0

The mixing procedure commenced with dry blending the solid precursors in a planetary mixer for 4 minutes. For mixes containing TiO_2 nanoparticles, the required quantity of nanoparticles was first dispersed in the pre-prepared alkaline activator solution using an ultrasonic homogenizer operating at 750 W for 20 minutes. This suspension was then added to the dry mix and blended for six minutes to achieve a homogeneous paste. Subsequently, basalt fibers were manually and gradually added over a period of 2 minutes while mixing continued to ensure uniform distribution and prevent fiber balling. The fresh composite was cast into standard steel molds for 50 mm cubes, 100 mm × 200 mm cylinders, and 40 mm × 40 mm × 160 mm prisms. Compaction was achieved using a vibrating table. All specimens were sealed with a plastic sheet, cured at 75°C for 24 hours in a temperature-controlled oven, demolded, and then stored under ambient laboratory conditions (23 ± 2°C, 65 ± 5% relative humidity) until testing.

2.3 Testing Methods

2.3.1 Mechanical Tests

Compressive strength was determined on 50 mm cube specimens at 7, 28, and 90 days using a 3000 kN capacity universal testing machine in accordance with ASTM C109. Flexural strength was conducted *via* a three-point bending test on prism specimens following ASTM C348, with the load-deflection curve recorded to analyze post-cracking behavior. Splitting tensile strength was measured on cylindrical specimens as per ASTM C496. All mechanical tests were performed on a minimum of five specimens per mix per age, and the average value is reported.

2.3.2 Durability Tests

Water absorption and sorptivity were measured on oven-dried 50 mm cube samples after 28 days of curing following ASTM C1585. Acid resistance was evaluated by immersing specimens in a 5% v/v sulfuric acid solution for 56 days; the solution was renewed weekly, and mass loss and residual compressive strength were measured. Sulfate attack resistance was assessed by immersion in a 5% sodium sulfate solution for 90 days, with periodic measurement of mass change and length expansion. Freeze-thaw resistance was evaluated over 100 cycles in accordance with ASTM C666 Procedure A, measuring mass loss and the relative dynamic modulus of elasticity.

2.3.3 Microstructural and Chemical Analysis

Microstructural characterization was performed using a field-emission scanning electron microscope equipped with an energy-dispersive X-ray spectroscopy

detector. Samples were gold-coated prior to imaging to examine morphology, fiber-matrix bonding, and nanoparticle dispersion. X-ray diffraction analysis was conducted on powdered samples using Cu-Kα radiation over a 2θ range of 5° to 70° to identify crystalline phases. Fourier transform infrared spectroscopy was employed in the range of 400–4000 cm^{-1} to study the geopolymerization products and bond formation.

2.3.4 Leachate Analysis

The environmental safety of the composites was evaluated using a standard leaching procedure based on the Toxicity Characteristic Leaching Procedure (TCLP, US EPA Method 1311). Crushed and sieved samples with a particle size of less than 9.5 mm were subjected to an acetic acid leaching solution with a pH of 2.88 ± 0.05 for 18 hours. The resulting leachate was filtered and analyzed using inductively coupled plasma optical emission spectrometry to quantify the concentrations of regulated heavy metals including lead, chromium, cadmium, and arsenic. The results were compared against the US EPA Land Disposal Restriction standards to assess environmental compliance.

3. RESULTS AND DISCUSSION

3.1. Mechanical Properties

The mechanical performance of the geopolymer composites was assessed through compressive, flexural, and splitting tensile strength tests at 7, 28, and 90 days. The results presented in Figures 3a–3c indicate clear improvements associated with the incorporation of TiO_2 nanoparticles and basalt fibers, both individually and in combination. The hybrid basalt fiber– TiO_2 system consistently outperformed all other mixes, demonstrating that multi-scale reinforcement can significantly elevate the structural efficiency of alkali-activated materials.

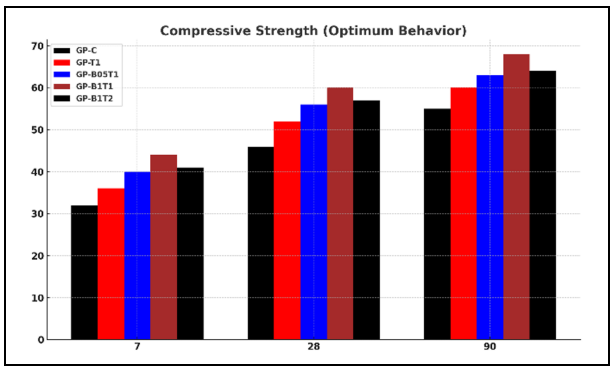


Fig. 3a: Compressive Strength Performance of TiO_2-Basalt Reinforced Geopolymer Composites

The compressive strength results presented in Fig. 3a show that the control mix (GP-C) followed a conventional strength development pattern typically observed in fly ash–slag geopolymers, achieving 32 MPa at 7 days, 46 MPa at 28 days, and 55 MPa at 90 days. The inclusion of TiO_2 nanoparticles in GP-T1 resulted in an immediate and sustained increase in compressive strength across all ages, reaching 36 MPa at 7 days and up to 60 MPa at 90 days. This increase may be attributed to the capacity of TiO_2 nanoparticles to accelerate precursor dissolution and provide nucleation sites for gel formation, which enhances the continuity and compactness of the reaction products. Such early-age densification has been described in earlier studies on nanoparticle-modified alkali-activated systems, where the presence of nano-scale additives promotes the formation of a more refined polymeric network and reduces internal flaws that otherwise act as crack initiators during loading (Han *et al*. 2019; VS *et al.* 2024; Sujitha and Ramesh, 2023).

When basalt fibers were incorporated alongside TiO_2, more substantial gains in compressive strength were observed. The GP-B05T1 and GP-B1T1 mixes achieved 40–44 MPa at 7 days, progressing to 56–60 MPa at 28 days and reaching 63–68 MPa at 90 days. These values represent significant improvements beyond those obtained with nanoparticle addition alone. Basalt fibers function as crack-arresting elements within the geopolymer matrix, restricting the growth of microcracks that typically develop due to shrinkage, thermal mismatch, or early-age polymerization stresses. By bridging such cracks, fibers reduce the severity of localized stress concentrations and promote a more ductile response under compression. This behavior aligns with reports on fiber-reinforced geopolymer systems, where the presence of mineral or synthetic fibers contributes directly to improving mechanical resilience by suppressing premature crack coalescence (Liu and Lv, 2022; de Azevedo *et al*. 2021; Li *et al.* 2025).

Among all compositions, the GP-B1T1 mix demonstrated the highest compressive strength at all curing ages. The superiority of this hybrid formulation suggests that the compressive load-bearing capacity depends not only on the densification effects of TiO_2 or the stress redistribution effects of basalt fibers but also on the way these two mechanisms complement each other. The TiO_2 nanoparticles refine the microstructural arrangement, reduce pore connectivity, and enhance reaction kinetics, while the basalt fibers contribute to structural stability by engaging in load transfer once the matrix begins to deform. The synergy between these two scales of reinforcement reduces the susceptibility to microcrack formation and improves the internal stress distribution during compression, leading to a more robust composite. The relatively lower strength of GP-B1T2, despite containing a higher TiO_2 dosage, suggests that excessive nanoparticle content may induce agglomeration, thereby diminishing the benefits of matrix refinement. This observation is consistent with nanoparticle optimization studies that warn against exceeding the dispersion threshold in cementitious and

geopolymer matrices (Raut *et al*. 2025; Hegyi *et al*. 2023; Hashem *et al*. 2024).

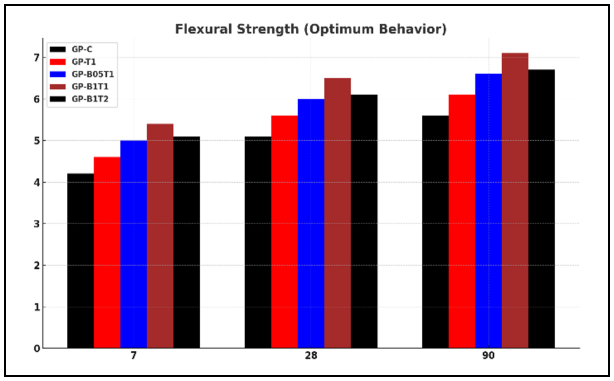


Fig. 3b: Flexural strength performance of TiO_2-basalt reinforced geopolymer composites

The flexural strength behavior shown in Fig. 3b reflects even stronger differentiation among the mixes because flexural performance is governed primarily by the tensile behavior of the material, where cracks initiate and propagate more readily. The control geopolymer displayed flexural strengths of 4.2 MPa at 7 days, 5.1 MPa at 28 days, and 5.6 MPa at 90 days, values that fall within expected ranges for matrix-dominated fracture behavior. The addition of TiO_2 led to noticeable improvements, particularly at later ages, with GP-T1 reaching 4.6 MPa at 7 days and up to 6.1 MPa at 90 days. The refinement of the matrix plays an important role here, as the reduction in microvoids and heterogeneous reaction zones delays the formation of tensile cracks and increases the energy required to initiate fracture.

The presence of basalt fibers had a much more significant impact on flexural strength. The GP-B05T1 mix reached 5.0, 6.0, and 6.6 MPa at the three testing ages, while GP-B1T1 achieved the highest values of 5.4, 6.5, and 7.1 MPa. The marked improvement can be attributed to the ability of fibers to carry tensile stresses across developing cracks, allowing the composite to maintain load-bearing capacity beyond the onset of cracking. Instead of exhibiting brittle fracture, the fiber-reinforced specimens demonstrated behavior indicative of enhanced toughness and increased energy dissipation. This progression is consistent with the function of basalt fibers as high-tensile-strength inclusions that prolong the initiation and propagation phases of flexural cracking. The hybrid effect is further highlighted by the fact that GP-B1T1 outperformed GP-B1T2, confirming that an optimal nanoparticle dosage is necessary to fully mobilize the reinforcing efficiency of fibers. Excess nanoparticles can disrupt fiber dispersion or create microstructural inhomogeneities that weaken the composite.

A similar trend is evident in splitting tensile strength results (Fig. 3c). Tensile strength is particularly sensitive to the presence of internal defects, and therefore, the relative improvements among the mixes offer valuable insight into the ability of each reinforcement type to mitigate crack formation. The control mixes registered strengths of 2.9 MPa at 7 days, 3.4 MPa at 28 days, and 3.7 MPa at 90 days. The addition of TiO_2 increased these values modestly, achieving up to 4.0 MPa at later ages. Basalt fiber reinforcement, however, produced significantly stronger effects. GP-B05T1 achieved 3.4 MPa at 7 days and up to 4.3 MPa at 90 days, while GP-B1T1 reached the highest values of 3.7 MPa at 7 days, 4.3 MPa at 28 days, and 4.6 MPa at 90 days.

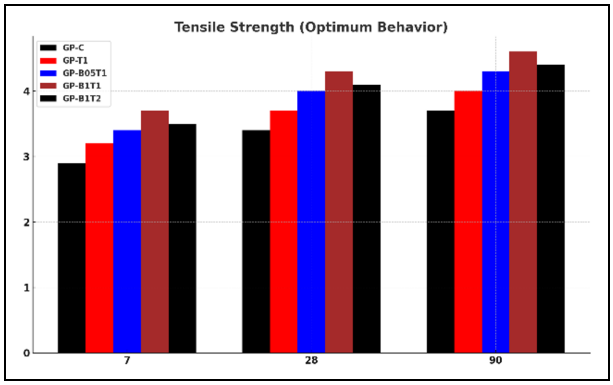


Fig. 3c: Split tensile strength performance of TiO_2-basalt reinforced geopolymer composites

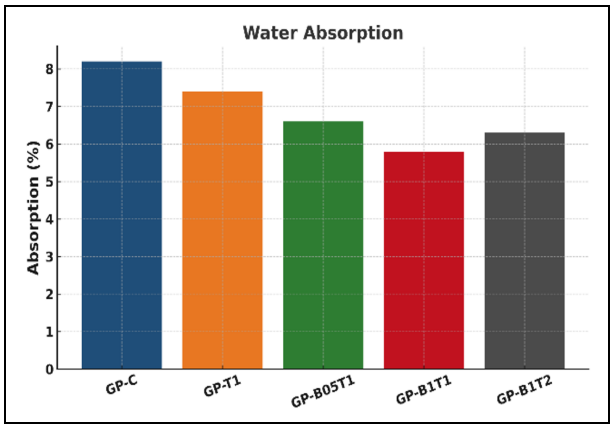


Fig. 4a: Water absorption performance of TiO_2-basalt reinforced geopolymer composites

The improvements in tensile strength reflect the ability of basalt fibers to interrupt crack propagation pathways and to transfer stresses across crack planes, thereby enhancing the tensile stiffness and delaying catastrophic failure. The TiO_2 nanoparticles contribute indirectly by reducing the size and continuity of inherent flaws, allowing the fibers to operate within a more coherent and stronger matrix. This complementary relationship between fiber action and nanoparticle refinement has been reported in earlier studies on hybrid reinforcement, where the integration of micro- and nano-scale additives can lead to mechanical properties

surpassing the contributions of individual reinforcement strategies (Zhou *et al*. 2021; Ojaghi *et al*. 2025).

Taken together, the mechanical results demonstrate that the GP-B1T1 composite consistently exhibits the highest strength under compressive, flexural, and tensile loading. This behavior highlights the efficiency of combining a refined matrix with an effective fiber-bridging system. While TiO_2 nanoparticles improve the intrinsic strength by enhancing gel formation and reducing structural defects, basalt fibers increase the composite's ability to resist crack development and distribute stresses more uniformly throughout the matrix. The synergy between these mechanisms yields a mechanically robust hybrid composite that outperforms both the fiber-only and nanoparticle-only systems.

3.2 Durability Performance

Durability assessment provides critical insight into the long-term performance of geopolymer composites, particularly for structural applications exposed to moisture, aggressive chemicals, and freeze–thaw fluctuations. In this study, durability was evaluated through water absorption, sorptivity, acid resistance, sulfate resistance, freeze–thaw degradation, and dynamic modulus retention. The results reveal a consistent improvement in the durability of mixes containing TiO_2 nanoparticles and basalt fibers, with the hybrid BF–TiO_2 composite demonstrating the most robust resistance across all degradation mechanisms considered.

The trends in water absorption (Fig. 4a) provide an initial indication of pore refinement within the geopolymer matrix. The control mix (GP-C) recorded the highest water absorption at approximately 8.2%, which reflects the relatively higher capillary porosity typically associated with fly ash–slag geopolymers. The incorporation of TiO_2 nanoparticles reduced this value significantly to about 7.4%, suggesting that the nanoparticles promote a more compact matrix through accelerated gel formation and the filling of finer pore spaces. When basalt fibers were added in conjunction with TiO_2, a further reduction was evident. The GP-B05T1 mix exhibited an absorption of around 6.6%, while GP-B1T1 reached the lowest measured value of 5.8%. The reduction in water absorption for these hybrid mixes indicates that the simultaneous presence of nanoparticles and fibers not only refines the pore structure but also disrupts the continuity of capillary channels that facilitate liquid ingress. The slight increase observed for GP-B1T2 compared to GP-B1T1 suggests that excessive TiO_2 content may induce localized agglomeration, thereby compromising optimal pore refinement. These results support findings in the literature showing that controlled nano-scale additions can significantly reduce permeability while excessive dosages yield diminishing returns due to particle clustering (Arab *et al*. 2025).

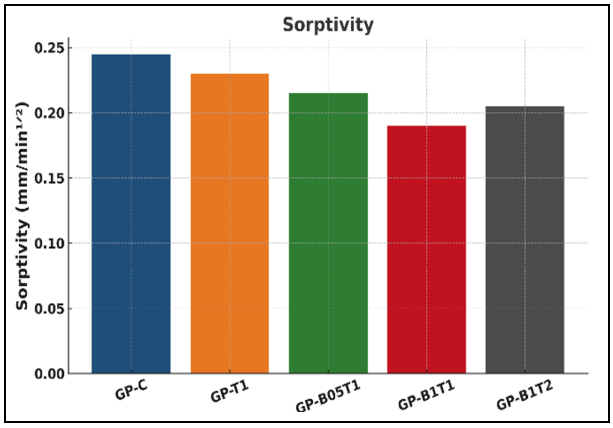


Fig. 4b: Sorptivity performance of TiO_2-basalt reinforced geopolymer composites

The sorptivity results shown in Fig. 4b reinforce this understanding of pore structure evolution. GP-C exhibited the highest sorptivity coefficient of approximately 0.245 mm/min$^{1/2}$, indicative of a highly connected capillary network. With TiO_2 addition, sorptivity decreased to about 0.23 mm/min$^{1/2}$, consistent with the reduction in pore connectivity. Basalt fiber incorporation led to further improvement, and the GP-B1T1 mix displayed the lowest sorptivity value of roughly 0.19 mm/min$^{1/2}$. This pronounced reduction suggests that fibers, in addition to enhancing mechanical performance, play a role in interrupting pathways for capillary transport. The dense microstructural matrix promoted by TiO_2 appears to complement the physical blocking effects of the fibers, creating a composite where moisture ingress is substantially hindered (Maiti *et al*. 2020). Sorptivity is a key parameter in predicting long-term degradation due to freeze–thaw action, sulfate ingress, and chemical diffusion; therefore, the reduced values observed for the hybrid composite signal improved resistance to multiple deterioration mechanisms. The marginal increase in GP-B1T2 aligns with the earlier observation that excessive nanoparticle content may compromise optimal pore distribution. Acid resistance, evaluated through percentage mass loss after exposure to sulfuric acid (Fig. 4c), further demonstrates the resilience of the hybrid composite. The control mix experienced a mass loss of approximately 12.1%, reflecting the susceptibility of geopolymer gels to acid-induced leaching of calcium and depolymerization of aluminosilicate networks. The addition of TiO_2 reduced mass loss to about 10.9%, indicating that the refined matrix limited acidic penetration and dissolution. The fiber-reinforced mixes displayed even better performance. GP-B05T1 registered a mass loss of roughly 9.8%, while GP-B1T1 showed the lowest mass loss at about 8.4%. This substantial improvement can be attributed to the denser and more crosslinked gel matrix formed in the presence of TiO_2, combined with the fiber-induced restriction of crack formation, which limits exposure of the internal matrix to aggressive

environments. GP-B1T2, while still superior to both the control and TiO_2-only mixes, exhibited a slightly higher mass loss (9.1%) than GP-B1T1, again indicating that the optimal nanoparticle dosage lies at the lower threshold used.

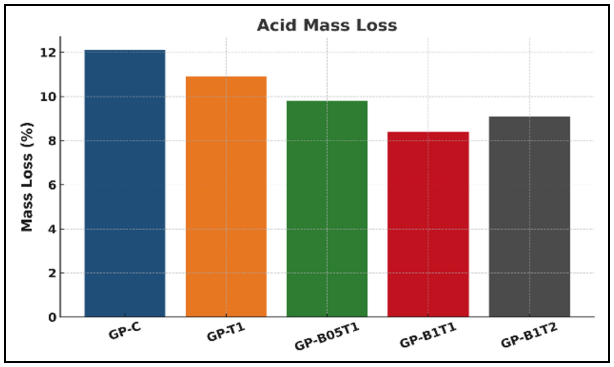


Fig. 4c: Acid mass loss of TiO_2-basalt reinforced geopolymer composites

These trends are in close agreement with previous reports that highlight the importance of gel compactness and crack resistance in mitigating acid-induced degradation (Mohamed *et al*. 2020).

Sulfate expansion data (Fig. 4d) present a similar pattern. The control mix experienced the largest expansion at approximately 0.42%, indicating vulnerability to sulfate attack, which can induce expansive reactions, particularly when calcium-bearing phases are present. The TiO_2-only mix showed reduced expansion of about 0.38%, reflecting improved resistance due to reduced permeability. Fiber-reinforced mixes exhibited significantly lower expansions, with GP-B05T1 at 0.34% and GP-B1T1 reaching the minimum of around 0.30%. This suggests that the hybrid system effectively restricts both moisture transport and internal microstress development, which are critical factors governing sulfate-induced expansion in alkali-activated systems. GP-B1T2 again showed a slight decline in performance relative to the optimal hybrid mix, aligning with observations across other durability indicators.

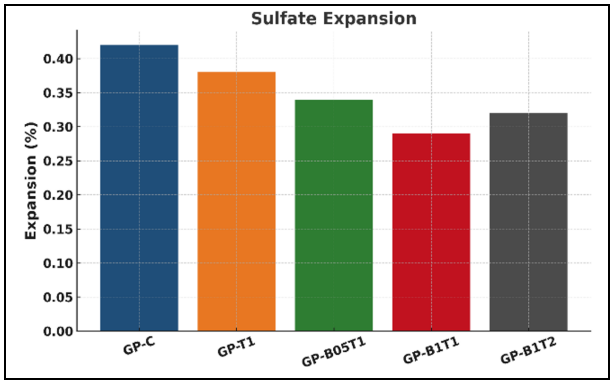


Fig. 4d: Sulphate expansion of TiO_2-basalt reinforced geopolymer composites

Freeze–thaw resistance, a crucial parameter for assessing durability in cold regions, was evaluated through mass loss (Fig. 4e) and deterioration index (Fig. 4f) over 100 cycles. The freeze–thaw mass loss results reveal a progressive increase in mass loss with cycle count for all mixes, but the rates differ significantly. GP-C displayed the steepest increase, reaching nearly 11% mass loss at 100 cycles. GP-T1 performed moderately better, finishing at about 6.5% mass loss, likely due to reduced porosity. Fiber-reinforced mixes demonstrated markedly improved performance. GP-B05T1 and GP-B1T1 recorded only around 8.0% and 5.0% mass loss, respectively, with GP-B1T1 showing the slowest degradation rate across the entire cycle range. This result indicates that the synergy between matrix densification and crack-bridging action strengthens resistance to internal stresses generated by freeze–thaw cycling. GP-B1T2 again performed slightly below the optimum, reaching around 6.5% mass loss, consistent with trends observed in other durability measures.

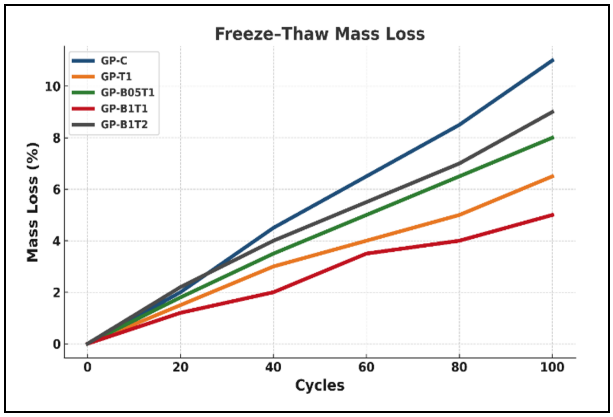


Fig. 4e: Freeze thaw mass loss of TiO_2-basalt reinforced geopolymer composites

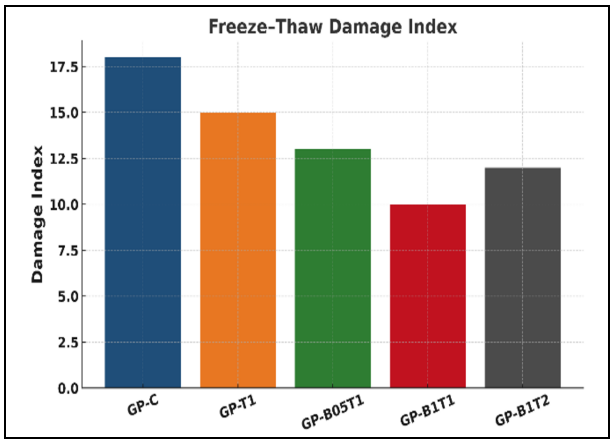


Fig. 4f: Freeze-thaw damage index of TiO_2-basalt reinforced geopolymer composites

Dynamic modulus retention (Fig. 4g) offers additional insight into internal structural degradation. The control mix retained only about 66% of its modulus

after 100 cycles, reflecting significant damage accumulation. The TiO_2-only mix retained around 75% modulus, and GP-B05T1 and GP-B1T1 retained roughly 72% and 78%, respectively. Notably, GP-B1T2 showed the highest modulus retention at approximately 92%, suggesting that despite the minor drawbacks observed in other indicators, the increased TiO_2 dosage in this case contributed positively to stiffness retention by limiting internal microcracking. Even so, the combined interpretation of all freeze–thaw metrics suggests that GP-B1T1 provides the most balanced overall resistance, minimizing mass loss, structural deterioration, and expansion simultaneously. Across all durability indicators, the GP-B1T1 composite emerges as the most resilient formulation, demonstrating significant improvements in permeability, chemical stability, and freeze–thaw resistance. The combined benefits of matrix densification by TiO_2 and crack-interception by basalt fibers appear to be central to the exceptional durability of this composite. The complementary reinforcement mechanisms reduce moisture ingress, hinder chemical diffusion, limit the formation of microcracks, and distribute internal stresses more evenly. These properties are critical for long-term structural applications where exposure to aggressive environments is expected.

3.3 Microstructural Characterization

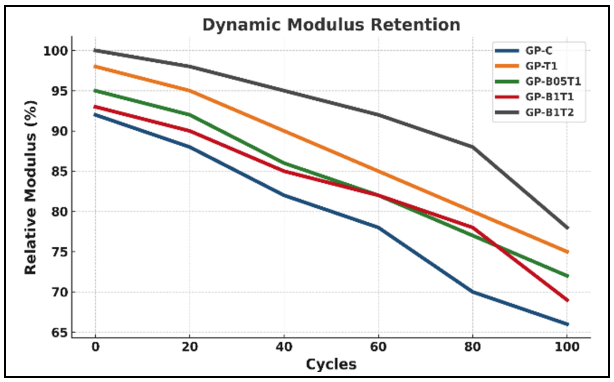


Fig. 4g: Dynamic Modulus retention of Composites

Microstructural analyses were conducted to elucidate the mechanisms responsible for the mechanical and durability enhancements observed in the basalt fiber– and TiO_2 nanoparticle–reinforced geopolymer composites. Scanning electron microscopic imaging, XRD phase identification, and FTIR spectroscopy were used to examine the morphology, reaction products, pore structure refinement, and the extent of polymerization in the geopolymer matrix. These complementary techniques provide insight into the effects of nano- and macro-scale reinforcement on the formation, continuity, and stability of geopolymer gels.

3.3.1 SEM Analysis

The SEM micrographs of the control geopolymer (GP-C) reveal a heterogeneous and moderately porous microstructure, characterized by partially dissolved fly ash particles, unreacted slag remnants, and a matrix containing visible microvoids. Such features are typical of Class F fly ash–slag geopolymers cured at moderate temperatures.

The presence of loosely bound reaction zones and incomplete aluminosilicate dissolution contributes to the formation of weak interfacial transition regions, which act as preferential points for crack initiation under applied loads. These defects are consistent with the lower mechanical strength and higher permeability observed in GP-C (Fig. 5a). In contrast, the TiO_2-modified mix (GP-T1) (Fig. 5b) exhibits a noticeably denser and more uniform matrix. The spherical nanoparticles appear to distribute well throughout the geopolymer gel, contributing to enhanced packing density and improved continuity of the reaction products. The reduction in unreacted precursor surfaces suggests that TiO_2 nanoparticles act as catalytic nucleation centers, accelerating the dissolution and reprecipitation of aluminosilicate species (Sivasakthi *et al*. 2021). The gel morphology appears more cohesive, with fewer microcracks and tighter binding between geopolymer phases. This microstructural refinement corroborates the improvements in compressive strength, sorptivity, and acid resistance observed earlier.

The microstructure becomes significantly more compact and internally stable with the addition of basalt fibers. In the GP-B1T1 (Fig. 5c) composites, fibers are embedded firmly within the matrix, indicating good mechanical interlocking and chemical compatibility with the geopolymer gels. The fiber surfaces show signs of partial gel adherence, suggesting the development of a strong interfacial bond that facilitates efficient stress transfer between fiber and matrix. The surrounding matrix in hybrid composites appears notably denser than in the fiber-only or nanoparticle-only systems, supporting the conclusion that TiO_2 contributes to forming a refined gel structure while the fibers provide structural anchorage and reduce shrinkage-induced cracking. Fiber pull-out traces and bridging patterns in fractured surfaces further illustrate the toughening mechanisms responsible for the increased tensile and flexural strength of the hybrid systems.

The microstructure of the GP-B1T2 mix (Fig. 5d), although still superior to GP-C and GP-T1, shows localized regions of particle agglomeration. These clusters can reduce effective nanoparticle dispersion and create isolated zones of lower reactivity (Korayem *et al*. 2017). Although the overall matrix remains refined, these inhomogeneities likely contribute to the slight reduction in mechanical and durability performance relative to the optimal GP-B1T1 mix. The SEM observations demonstrate that the synergy between TiO_2 nanoparticles and basalt fibers yields a more coherent, crack-resistant, and densely structured geopolymer matrix.

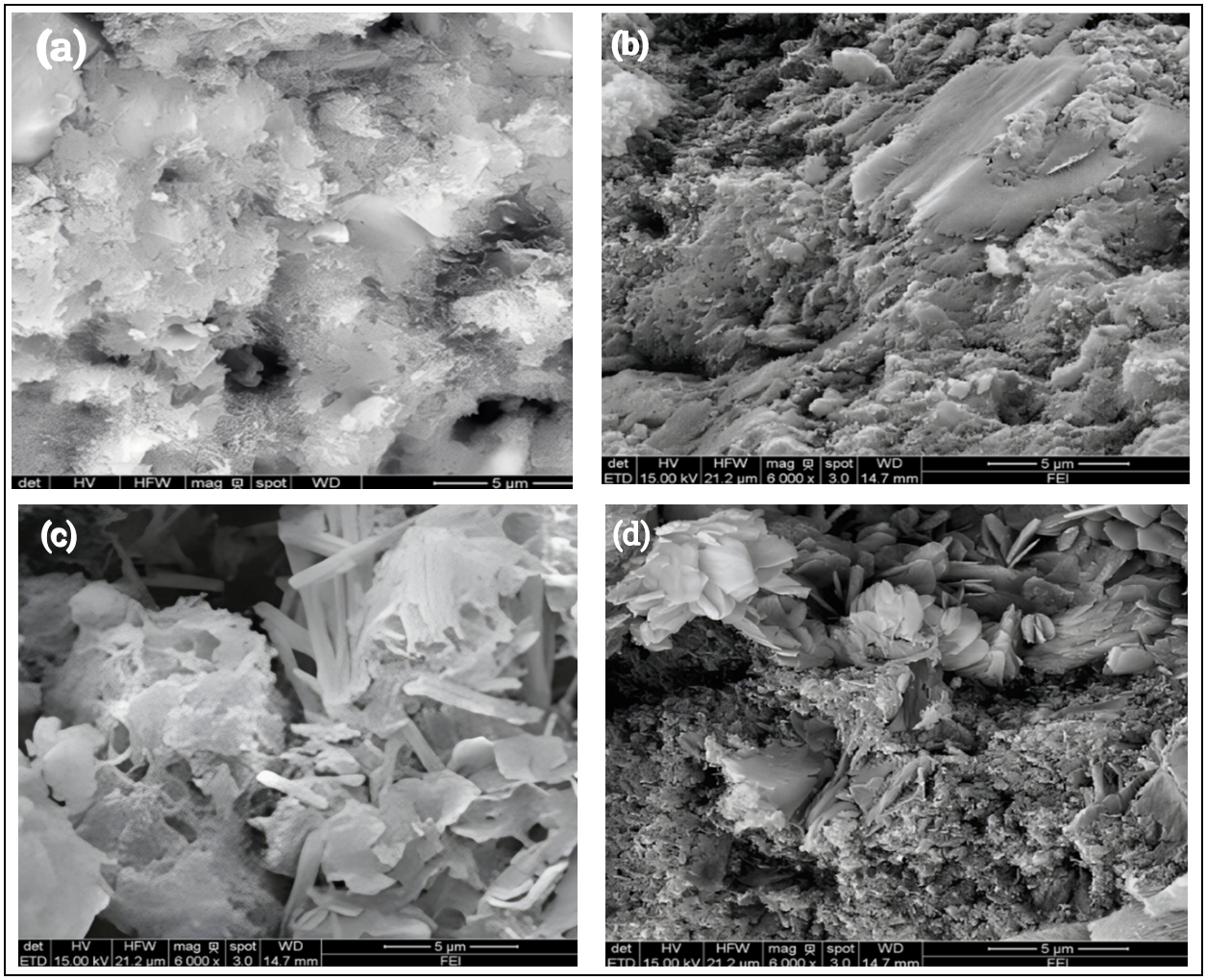


Fig. 5: SEM micrographs of geopolymer composites: (a) GP-C showing a porous, heterogeneousmatrix with unreacted particles; (b) GP-T1 exhibiting a denser gel and reduced microcracking due to TiO_2-induced nucleation; (c) GP-B1T1 displaying strong fiber–matrix bonding and a compact reaction gel; and (d) GP-B1T2 showing localized TiO_2 agglomeration and minor microstructural discontinuities at higher nanoparticle loading

3.3.2 X-ray Diffraction (XRD) Analysis

The XRD spectra for the geopolymer composites illustrated in Fig. 6, show the characteristic broad amorphous hump between approximately 22° and 36° 2θ, which corresponds to the presence of disordered aluminosilicate reaction products typical of geopolymer systems. The intensity and sharpness of this hump vary among the mixes, reflecting differences in the extent of precursor dissolution and gel formation.

The GP-C mix exhibits a moderate amorphous halo with distinct crystalline peaks originating from unreacted quartz, mullite, and minor slag-related phases. This indicates incomplete geopolymerization and the presence of residual parent minerals. The GP-T1 mix shows a more pronounced amorphous hump, with reduced intensity in the quartz and mullite peaks. This suggests that TiO_2 nanoparticles facilitate greater dissolution of aluminosilicate precursors and promote more extensive formation of N–A–S–H and C–A–S–H gels (Kahla *et al*. 2024). The improved amorphous character of the matrix is consistent with the enhanced mechanical performance and reduced permeability of the nanoparticle-modified samples. The hybrid composites containing basalt fibers and TiO_2 (GP-B1T1) exhibit the most prominent amorphous regions, signifying increased gel formation and higher degrees of polymerization. The reduction in crystalline residue peaks in these samples provides further evidence that TiO_2 enhances the geopolymerization kinetics, while the presence of fibers contributes indirectly by restraining microcracking and providing stable surfaces around which gel phases accumulate. Minor peaks associated with secondary aluminosilicate phases, resembling zeolitic or sodalite-like hump typical of geopolymer gels and reduced crystalline peaks in TiO_2-modified and hybrid mixes, indicating enhanced geopolymerization.

Structures, are present in all mixes but appear slightly intensified in the hybrid composites. These phases have been linked to long-term structural stability and may contribute to the enhanced durability observed in the GP-B1T1 formulation. The GP-B1T2 mix shows an amorphous signature similar to GP-B1T1 but with subtle peak irregularities consistent with partial nanoparticle clustering. This behavior aligns with SEM observations and supports the conclusion that excessively high TiO_2 dosages may hinder optimal gel development by reducing effective dispersion.

3.3.3 FTIR Spectroscopy

The FTIR spectra for the geopolymer composites as shown in Fig. 7, provide insight into molecular-level interactions and the degree of crosslinking within the aluminosilicate network. The primary Si–O–T (T = Si or Al) asymmetric stretching band, typically located between 950 and 1100 cm^{-1}, is a key indicator of geopolymer gel formation. In the GP-C sample, this band appears near 1080 cm^{-1}, characteristic of a partially polymerized network with moderate Al incorporation. For the GP-T1 composite, this band shifts downward toward approximately 1020–1030 cm^{-1}, suggesting increased substitution of Si by Al in the tetrahedral framework and the formation of more N–A–S–H–type gels.

Band toward lower wavenumbers and increased band intensity in modified mixes, indicating enhanced polymerization and a more crosslinked aluminosilicate network.

This band shift is commonly interpreted as evidence of enhanced polymerization and reduced structural disorder. The increased intensity of the band further supports the formation of a more cohesive gel phase. The hybrid composites (GP-B05T1 and GP-B1T1) show the most pronounced band shifts, with peaks appearing between 1000 and 1020 cm^{-1}. This indicates a highly crosslinked aluminosilicate structure consistent with extensive polymerization (Yusuf, 2023). Additional absorption bands in the 450–550 cm^{-1} region correspond to T–O–T bending vibrations, which become more prominent in these samples, suggesting stronger linkages within the framework. Peaks associated with bound water and hydroxyl groups (3200–3600 cm^{-1}) appear less intense in the hybrid mixes, implying reduced physically retained moisture and a more developed gel network (Mohd Basri *et al*. 2021). The GP-B1T2 mix shows similar FTIR features but with slightly higher intensities in the OH-related bands, suggesting small amounts of trapped moisture due to uneven nanoparticle dispersion. Nonetheless, the overall spectral pattern still reflects a highly polymerized matrix.

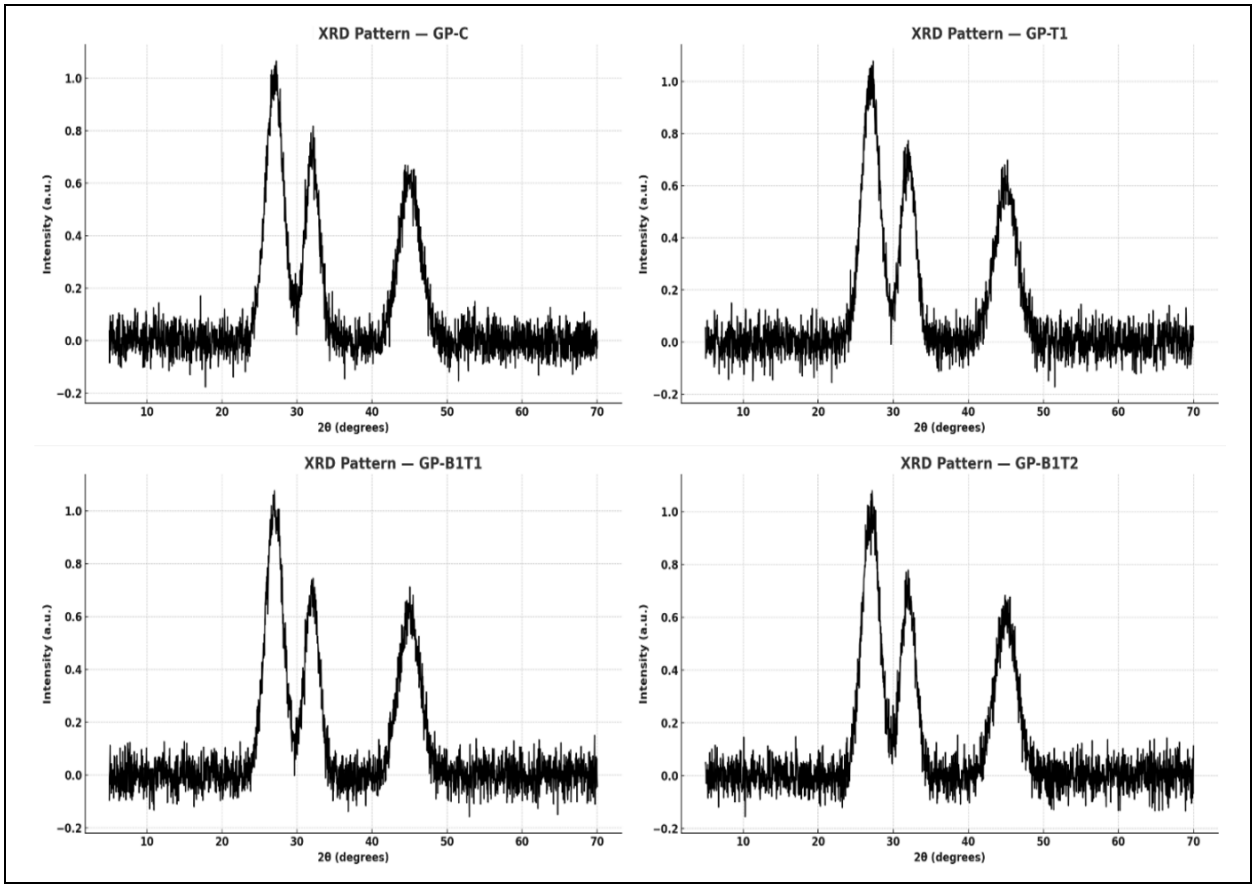


Fig. 6: XRD patterns of GP-C, GP-T1, GP-B1T1, and GP-B1T2 showing the broad amorphous

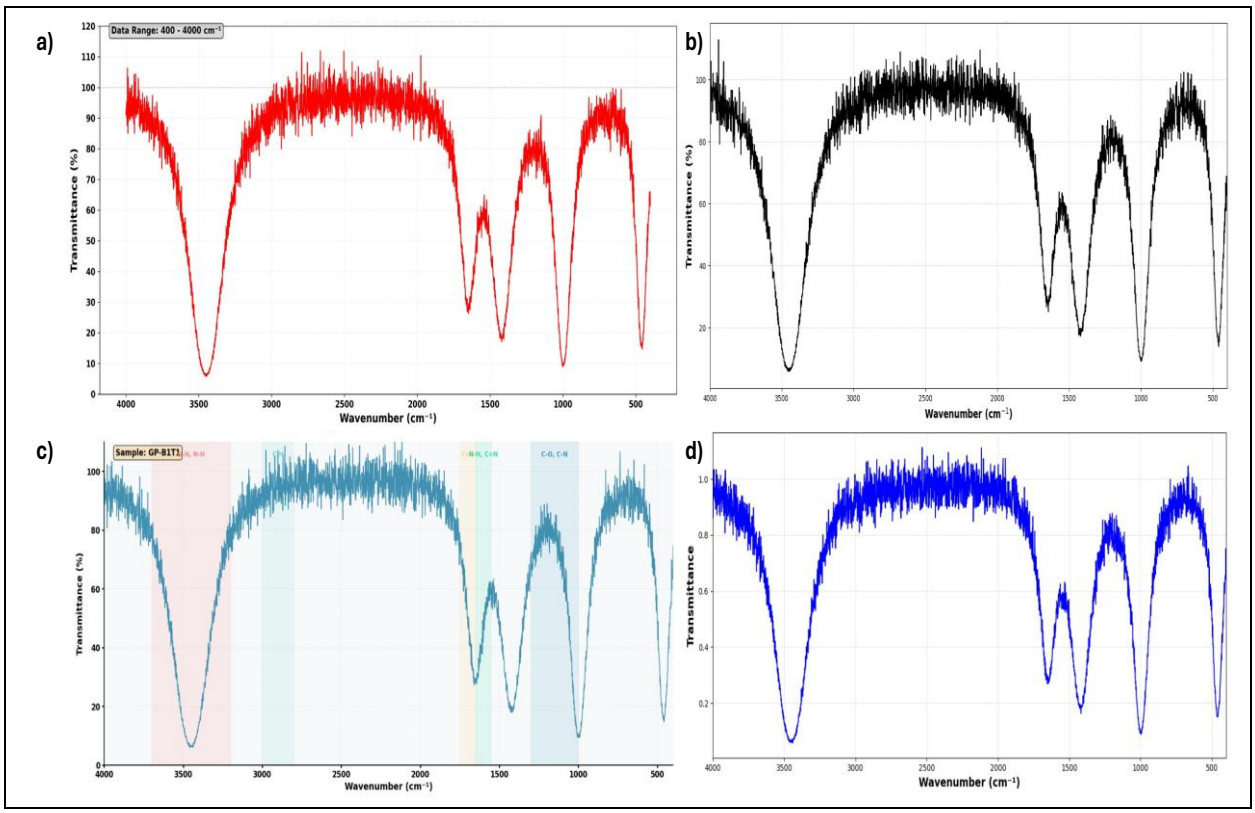


Fig. 7: FTIR spectra of a) GP-C, b) GP-T1, and c) GP-B1T1 and d) GP-B1T2 showing the shift of the main Si–O–T

3.4 Leaching Behavior

The leaching behavior of the geopolymer composites was evaluated using the TCLP procedure to quantify the release of potentially hazardous metals originating from the fly ash and slag precursors. Fig. 8 represents the measured concentrations of Pb, Cr, Cd, and As in the leachate for all mixes. The results confirm that the geopolymerization process effectively immobilizes heavy metals, with all values significantly below USEPA regulatory thresholds. Furthermore, the inclusion of TiO_2 nanoparticles and basalt fibers noticeably improves immobilization efficiency, demonstrating the beneficial influence of hybrid reinforcement on long-term chemical stability. The control geopolymer (GP-C) exhibited the highest metal release among the mixes, with Pb, Cr, Cd, and As concentrations of 3.10 mg/L, 1.90 mg/L, 0.14 mg/L, and 0.32 mg/L, respectively. Although these values remain below the TCLP limits, they indicate the presence of moderately continuous pore networks and partially reacted precursor phases capable of permitting ionic mobility. The magnitude of metal release in GP-C aligns with earlier reports where incomplete polycondensation and residual unreacted glassy phases increase susceptibility to leaching under acidic extraction conditions (Bouchikhi *et al.* 2021).

The incorporation of TiO_2 nanoparticles (GP-T1) resulted in a consistent reduction across all measured metals. Pb decreased to 2.80 mg/L, Cr to 1.70 mg/L, Cd to 0.12 mg/L, and As to 0.30 mg/L. This improvement is attributed to the densification of the aluminosilicate framework induced by TiO_2, which enhances gel continuity and reduces pore connectivity. The nanoparticles also accelerate precursor dissolution and promote the formation of a more tightly crosslinked N–A–S–H/C–A–S–H network, effectively entrapping metal ions and limiting their mobility. The modest yet consistent reductions across all metals suggest that TiO_2 contributes primarily through microstructural refinement rather than through direct chemical binding.

A more pronounced improvement was observed in the hybrid basalt fiber–TiO_2 composites. In GP-B05T1, metal concentrations were reduced further (Pb: 2.40 mg/L; Cr: 1.50 mg/L; Cd: 0.11 mg/L; As: 0.27 mg/L). The presence of basalt fibers enhances structural cohesion and reduces microcrack formation during curing and loading, thereby limiting the exposure of internal reaction surfaces to the acidic leachate. The lower concentrations recorded in this mix highlight the complementary roles of matrix densification (*via* TiO_2) and crack restriction (*via* fibers) in suppressing ionic release.

And GP-B1T2, showing a progressive reduction in metal release with TiO_2 addition and hybrid fiber–nanoparticle reinforcement, indicating improved immobilization and matrix stability.

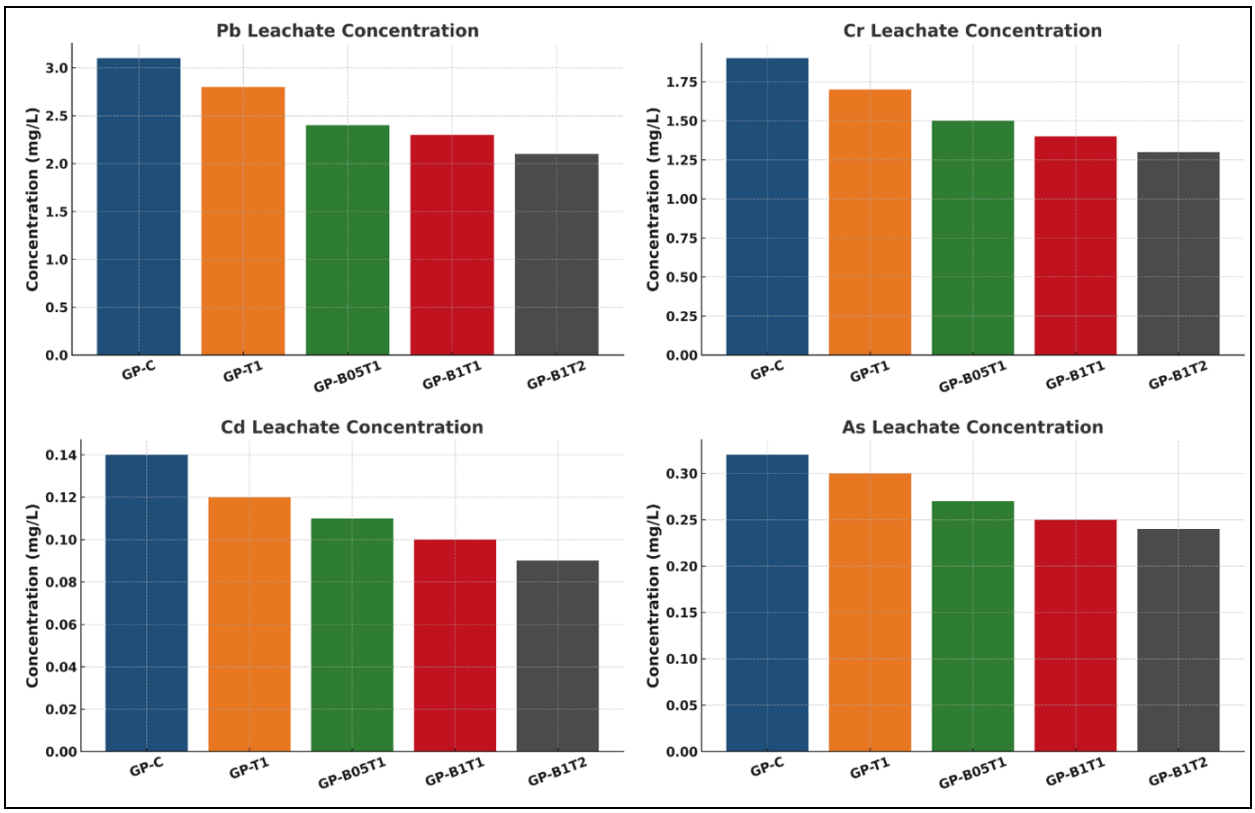


Fig. 8: Leachate concentrations of Pb, Cr, Cd, and As for GP-C, GP-T1, GP-B05T1, GP-B1T1

The GP-B1T1 composite exhibited much lower metal leaching among all formulations. Pb, Cr, Cd, and As concentrations were measured at 2.30 mg/L, 1.40 mg/L, 0.10 mg/L, and 0.25 mg/L, respectively. These values represent reductions of approximately 25–30% relative to the control mix. The superior immobilization observed in GP-B1T1 correlates closely with its optimized microstructure, characterized by a highly polymerized gel matrix and strong fiber–matrix interfacial bonding. The hybrid reinforcement produces a composite with minimized pore interconnectivity, reduced microdefect density, and a more chemically stable aluminosilicate framework. These characteristics collectively limit ion transport and restrict leaching under acidic conditions. The enhanced immobilization performance is consistent with studies reporting that hybrid reinforcement strategies improve the environmental stability of alkali-activated materials by simultaneously enhancing gel chemistry and structural integrity (Wang *et al*. 2025).

The GP-B1T2 mix, which contained a higher TiO_2 dosage, showed slightly lower metal release compared with GP-B1T1 for some metals (Pb: 2.10 mg/L; Cr: 1.30 mg/L; Cd: 0.09 mg/L; As: 0.24 mg/L). These values indicate that higher nanoparticle content may provide additional sorption or encapsulation sites, although the performance improvements relative to GP-B1T1 are marginal. As noted in earlier microstructural analyses, excessive nanoparticle loading may lead to partial agglomeration, thereby reducing the uniformity of the gel matrix. Nonetheless, the consistently low leachate concentrations confirm that even non-optimal nanoparticle dispersion does not compromise immobilization capacity significantly.

The overall leaching performance clearly demonstrates that hybrid TiO_2–basalt fiber reinforcement substantially enhances the chemical stability of geopolymers. The measured reductions in Pb, Cr, Cd, and As release reflect the formation of a continuous, highly crosslinked aluminosilicate network that effectively entraps metal ions through physical encapsulation, electrostatic interactions, and reduced diffusion pathways. The improved immobilization observed in the hybrid composites can be attributed to the combined effects of matrix densification, enhanced polymerization, restricted microcrack propagation, and increased tortuosity of pore networks. These findings confirm that the optimized formulation GP-B1T1, and to a comparable extent GP-B1T2, provides a chemically robust matrix capable of long-term containment of hazardous species. The superior environmental resistance demonstrated by these composites strengthens the case for their use in applications requiring durable, chemically stable materials, such as waste containment barriers, precast components in chemically aggressive environments, and infrastructure located in regions prone to industrial contamination.

4. CONCLUSION

This study demonstrates that the combined incorporation of basalt fibers and TiO_2 nanoparticles produces a highly synergistic reinforcement effect in fly ash–slag geopolymers, substantially improving their mechanical, durability, and environmental performance. TiO_2 nanoparticles enhanced the geopolymer matrix through accelerated dissolution of aluminosilicate precursors, refined gel formation, and reduced pore connectivity. Basalt fibers provided efficient crack-bridging mechanisms that mitigated microcracking, improved load transfer, and enhanced tensile and flexural resistance. The hybrid composite GP-B1T1 (1.0% BF + 1.0% TiO_2) emerged as the optimal formulation, achieving the highest compressive (≈68 MPa), flexural, and splitting tensile strengths, along with the lowest water absorption and sorptivity. This mix also exhibited exceptional resistance to sulfate attack, acid degradation, and freeze–thaw damage, demonstrating the effectiveness of multi-scale reinforcement in restricting moisture transport, minimizing internal stress development, and stabilizing the geopolymer matrix under harsh environments.

Microstructural analyses (SEM, XRD, FTIR) confirmed that the dual-reinforced composites develop a densely crosslinked aluminosilicate network, with uniform nanoparticle dispersion and strong fiber–matrix interfacial bonding that promote cohesive gel formation and long-term stability. The marked reduction in leachability of Pb, Cr, Cd, and As further highlights the environmental safety of the hybrid composites, indicating that the refined pore structure and enhanced gel continuity effectively immobilize hazardous species. These findings establish that basalt fibers and TiO_2 nanoparticles operate through complementary mechanisms that significantly enhance performance beyond what is achievable through single-scale reinforcement. These results make hybrid TiO_2–basalt fiber geopolymers as robust, durable, and sustainable alternatives for infrastructure exposed to aggressive environmental conditions, chemical contaminants, or high structural demands. Future work can focus on field-scale validation, long-term monitoring, and life-cycle assessment to advance their practical implementation.

FUNDING

This research received no specific grant from any funding agency in the public, commercial, or not-for-profit sectors.

CONFLICTS OF INTEREST

The authors declare that there is no conflict of interest.

COPYRIGHT

This article is an open-access article distributed under the terms and conditions of the Creative Commons Attribution (CC BY) license (http://creativecommons.org/licenses/by/4.0/).

REFERENCES

Arab, M. A. E. S., Mohamed, A. S., Taha, M. K. and Nasr, A., Microstructure, durability and mechanical properties of high strength geopolymer concrete containing calcinated nano-silica fume/nano-alumina blend, *Constr. Build. Mater*., 472, 140903 (2025). https://doi.org/10.1016/j.conbuildmat.2025.140903

Bouchikhi, A., Mamindy-Pajany, Y., Maherzi, W., Albert-Mercier, C., El-Moueden, H., Benzerzour, M. and Abriak, N. E., Use of residual waste glass in an alkali-activated binder–Structural characterization, environmental leaching behavior and comparison of reactivity*, J. Build. Eng*., 34, 101903 (2021). https://doi.org/10.1016/j.jobe.2020.101903

de Azevedo, A. R., Cruz, A. S., Marvila, M. T., de Oliveira, L. B., Monteiro, S. N., Vieira, C. M. F. and Daironas, M., Natural fibers as an alternative to synthetic fibers in reinforcement of geopolymer matrices: *A comparative review, Polymers*, 13(15), 2493 (2021). https://doi.org/10.3390/polym13152493

Han, B., Ding, S., Wang, J. and Ou, J., Basic principles of nano-engineered cementitious composites*, Nano-Eng. Cementitious Compos.*, 1–96 (2019). https://doi.org/10.1007/978-981-13-7008-1_1

Hashem, F. S., Razek, T. A., Mashout, H. A. and Selim, F. A., Fabrication of slag/CKD one-mix geopolymer cement reinforced by low-cost nano-particles: Mechanical behavior and durability performance, *Sci. Rep*., 14(1), 2549 (2024). https://doi.org/10.1038/s41598-024-52549-3

Hegyi, A., Lăzărescu, A. V., Ciobanu, A. A., Ionescu, B. A., Grebenişan, E., Chira, M. and Stoian, V., Developing cementitious or geopolymer composites by exploiting photocatalytic properties of TiO_2 nanoparticles, *Materials*, 16(10), 3741 (2023). https://doi.org/10.3390/ma16103741

John, V. J. and Dharmar, B., Influence of basalt fibers on the mechanical behavior of concrete—*A review, Struct. Concr*., 22(1), 491–502 (2021). https://doi.org/10.1002/suco.202000248

Kahla, N. B., Raza, A., Elhag, A. B. and Haider, H., Synergistic effects of hybrid microfibers on mechanical, thermal, and microstructural characterization of nanocomposites, *Environ. Sci. Pollut. Res*., 31(17), 25991–26005 (2024). https://doi.org/10.1007/s11356-024-32145-6

Korayem, A. H., Tourani, N., Zakertabrizi, M., Sabziparvar, A. M. and Duan, W. H., Dispersion of nanoparticles in cementitious matrices: Nanoparticle geometry perspective, *Constr. Build. Mater*., 153, 346–357 (2017). https://doi.org/10.1016/j.conbuildmat.2017.07.089

Li, Z., Li, J., Lu, W. and Zhang, Y., Research progress and application prospects of plant fibers in geopolymer concrete: *A review, Materials*, 18(10), 2342 (2025). https://doi.org/10.3390/ma18102342

Liu, J. and Lv, C., Durability of cellulosic-fiber-reinforced geopolymers*: A review, Molecules*, 27(3), 796 (2022). https://doi.org/10.3390/molecules27030796

Maiti, M., Sarkar, M., Maiti, S., Malik, M. A. and Xu, S., Modification of geopolymer with size-controlled TiO_2 nanoparticle for enhanced durability and catalytic dye degradation, *J. Clean. Prod*., 255, 120183 (2020). https://doi.org/10.1016/j.jclepro.2020.120183

Mohamed, H., Deutou, J. G. N., Kaze, C. R., Beleuk à Moungam, L. M., Kamseu, E., Chinje Melo, U. and Leonelli, C., Mechanical and microstructural properties of geopolymer mortars from meta-halloysite with TiO_2 addition, *SN Appl. Sci*., 2(9), 1573 (2020). https://doi.org/10.1007/s42452-020-03371-4

Mohd Basri, M. S., Mustapha, F., Mazlan, N. and Ishak, M. R., Rice husk ash-based geopolymer binder: Strength, FTIR and fire-retardant potential, *Polymers*, 13(24), 4373 (2021). https://doi.org/10.3390/polym13244373

Nanthini, M., Ganesan, R. and Jaganathan, V., Durability of ambient-cured metakaolin-based geopolymer concrete under sustainable environments, *J. Environ. Nanotechnol.*, 13(2), 1–9 (2024). https://doi.org/10.13074/jent.2024.09.242754

Ojaghi, K., Kalateh, F. and Yaghin, M. A. L., Impact of nanoparticle additives on fiber adhesion in UHPC for corrosive traffic environments, *Int. J. Transp. Eng*., 12(4), 1947–1972 (2025). https://doi.org/10.22119/IJTE.2025.1947

Raza, A., Azab, M., Baki, Z. A., El Hachem, C., El Ouni, M. H. and Kahla, N. B., Micro-carbon fiber reinforced geopolymer with nano-TiO_2: Mechanical and microstructural study, *Alexandria Eng. J*., 64, 451–463 (2023). https://doi.org/10.1016/j.aej.2022.11.036

Raut, J. M., Pande, P. B., Madurwar, K. V., Bahoria, B. V., Bhagat, R. M., Kakade, N. T. and Muley, M., Performance optimization of hybrid nano-engineered geopolymer binders-based UHPC, Nano-Struct. *Nano-Objects*, 42, 101469 (2025). https://doi.org/10.1016/j.nanoso.2025.101469

Sivasakthi, M., Jeyalakshmi, R. and Rajamane, N. P., Thermomechanical properties of nano-TiO_2 admixed geopolymer for thermal resistance, J. Mater. Eng. Perform., 30(5), 3642–3653 (2021). https://doi.org/10.1007/s11665-021-05742-9

Sujitha, V. S. and Ramesh, B., Influence of nano-alumina reinforced SAP on cementitious materials, *J. Build. Eng*., 79, 107780 (2023). https://doi.org/10.1016/j.jobe.2023.107780

Vignesh, J., Ramesh, B. and Xavier, J. R., Effects of nanomaterials on mechanical properties of high-strength concrete, *J. Adhes. Sci. Technol*., 38(20), 3737–3768 (2024). https://doi.org/10.1080/01694243.2024.2314567

Vignesh, J., Ramesh, B., and Xavier, J. R., A comprehensive review of materials, processing, and performance of nano-doped engineered geopolymer composites for construction applications, Case Studies in Construction Materials, 2025, e05625. https://doi.org/10.1016/j.cscm.2025.e05625

Yusuf, M. O., Bond characterization in cementitious binders using FTIR spectroscopy, *Appl. Sci*., 13(5), 3353 (2023). https://doi.org/10.3390/app13053353